ACS Catalysis

Research Article

pubs.acs.org/acscatalysis

Mechanistic Studies on the Switching from Ethylene Polymerization to Nonselective Oligomerization over the Triphenylsiloxy Chromium(II)/Methylaluminoxane Catalyst

Jialong Zhang,[†,⊥] Pengyuan Qiu,[†,‡,⊥] Zhen Liu,[†] Boping Liu,[*,†] Rami J. Batrice,[§] Mark Botoshansky,[§] and Moris S. Eisen[*,§]

[†]State Key Laboratory of Chemical Engineering, East China University of Science and Technology, Meilong Road 130, Shanghai 200237, People's Republic of China

[‡]Shanghai Research Institute of Petrochemical Technology, SINOPEC, 1658 Pudong Beilu, Shanghai, 201208, People's Republic of China

[§]Schulich Faculty of Chemistry, Technion-Israel Institute of Technology, Technion City, Haifa 32000, Israel

S *Supporting Information*

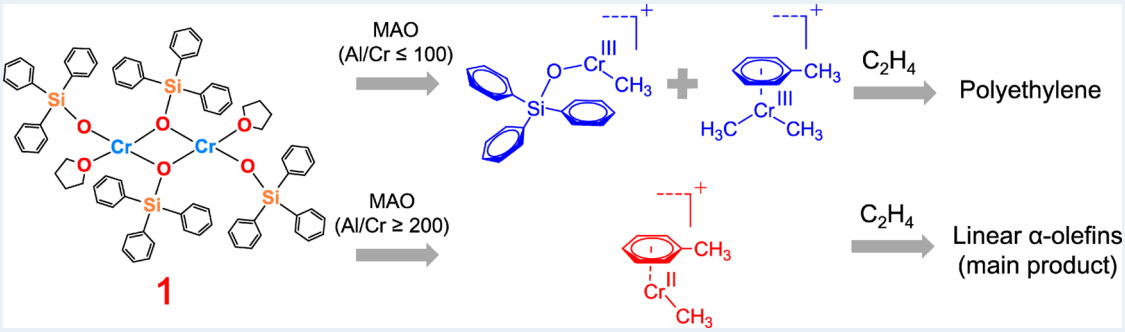

ABSTRACT: Our previous experimental report showed a switching behavior from ethylene polymerization to nonselective oligomerization by a novel triphenylsiloxy complex of chromium(II) $[(Ph_3SiO)Cr\cdot(THF)]_2(\mu\text{-}OSiPh_3)_2$ (**1**) together with methylaluminoxane (MAO) as a cocatalyst. In this work, combined experimental and computational studies were carried out to shed some light on the nature of the active species and their fascinating switching mechanism. The experimental results and DFT calculations suggested that (i) the chain propagation and chain transfer processes proceed via a Cossee−Arlman mechanism and β-hydrogen transfer to the chromium center, respectively; (ii) the trivalent cationic model $[(Ph_3SiO)Cr^{III}Me]^+$ and $[(\eta^6\text{-toluene})Cr^{III}Me_2]^+$, which could be generated by a disproportionation reaction, are the most plausible active species for ethylene polymerization, and the divalent cationic model $[(\eta^6\text{-toluene})Cr^{II}Me]^+$ might be responsible for ethylene nonselective oligomerization. A switching mechanism from ethylene polymerization to nonselective oligomerization in the **1**/MAO catalyst system was proposed on the basis of DFT calculations. These results may have useful implications for studying active species and the mechanism of transition-metal-catalyzed olefin polymerization and oligomerization.

KEYWORDS: *Phillips catalyst, ethylene polymerization, ethylene nonselective oligomerization, active species, switching mechanism, DFT calculations*

1. INTRODUCTION

As an important type of polymer, polyethylene is commonly utilized in various fields, such as containers, food/medical packaging, automotive/electrical components, and pipe materials, etc. Although ethylene is a kind of typically simple monomer, properties of the resulting polyethylene can be dramatically tuned by the polymerization catalysts employed. Among the transition-metal-based catalysts for ethylene polymerization, chromium-based catalysts are playing very important roles in the polyolefin industry.[1−6] The heterogeneous Phillips CrO_x/SiO_2 catalyst[7−10] and SiO_2-supported silylchromate UCC S-2 catalyst,[11] two of the most important industrial ethylene polymerization catalysts, are still producing about 10 million tons of high-density polyethylene (HDPE) each year all over the world.[10] In the meantime, the homogeneous chromium pyrrole-based ethylene trimerization catalyst was first successfully commercialized to provide comonomer grade 1-hexene for the production of value-added polyolefin products by the Chevron-Phillips Company in 2003.[12] Despite the great commercial success, basic understanding of the nature of the active species and polymerization/

Received: February 4, 2015
Revised: April 5, 2015
Published: April 30, 2015

DOI: 10.1021/acscatal.5b00240
ACS Catal. 2015, 5, 3562−3574

oligomerization mechanisms for these chromium-based catalysts is still controversial.

This situation has inspired the academic community to pay attention to their reaction mechanisms, the nature of active chromium species, and other factors that determine the activity and selectivity of various chromium-based catalysts for ethylene polymerization or oligomerization. In terms of reaction mechanisms, the nonredox Cossee−Arlman mechanism for ethylene polymerization is well established,[13,14] and the redox metallacycle mechanism for selective ethylene trimerization has been widely accepted.[15,16] However, it is not obvious which mechanism ethylene nonselective oligomerization follows, and both the nonredox Cossee−Arlman mechanism[17] and the redox metallacycle mechanism[18−20] have been proposed by different research groups. In addition, another main unsolved key issue in all the chromium-based catalyst systems is the metal oxidation states responsible for either ethylene oligomerization (selective and nonselective) or ethylene polymerization. The isolation of a series of switchable chromium-based catalysts has suggested that Cr(I) is active for ethylene-selective trimerization,[21−25] and Cr(II), for ethylene nonselective oligomerization and polymerization.[26] However, many research reports on chromium-based metallocene and non-metallocene catalysts have shown that the Cr(III) is responsible for ethylene polymerization, and the Cr(II) might be the active species for ethylene oligomerization over chromium-based metallocene and nonmetallocene catalysts.[27−31] As a matter of fact, it is difficult to clarify the relevance of the active oxidation states to their catalytic performance, considering the complexity of the multicomponent catalyst systems. Recently, Gambarotta and Duchateau et al. reported a series of chromium-based self-activating catalysts for ethylene polymerization and oligomerization,[32−35] which could provide significant information toward understanding the link between metal oxidation states and their catalytic behavior. For example, a previous study on pyrrole-based single-component catalyst systems has suggested that Cr(I) led to selective trimerization; Cr(II), to polymerization; and Cr(III), to nonselective oligomerization.[17] Moreover, by isolating reactive intermediates in the Cr-SNS (SNS= $RS(CH_2)_2N(H)(CH_2)_2SR$) catalyst system, it is realized that the Cr(II) complex may be reoxidized to Cr(III) by disproportionation,[35] suggesting that Cr(II) produces polyethylene or ethylene oligomers, whereas Cr(III) might form a redox couple with Cr(I), which is responsible for selective ethylene oligomerization.

In our recent report, a novel triphenylsiloxy complex of chromium(II) $[(Ph_3SiO)Cr\cdot(THF)]_2(\mu\text{-}OSiPh_3)_2$ (**1**) was successfully synthesized, and it is intriguing that complex **1** exhibits a switching behavior from ethylene polymerization to ethylene nonselective oligomerization with an increase in methylaluminoxane (MAO), as shown in Scheme 1.[36] Such a significant phenomenon implies that MAO plays an important role in this switching process, which deserves further basic research for the nature of active chromium species and their switching mechanism. A cationic $[Cr(I)(\eta^6\text{-arene})_2]^+$ sandwich complex was observed from the ESR spectrum in our previous work. However, this 17-electron sandwich complex is inactive for ethylene polymerization/oligomerization, and signals related to other chromium oxidation states which could be the real chromium species were not observed. In fact, for many transition-metal/MAO catalyst systems, experimental characterization of active catalytic species is very challenging because of its multitudinous complexity and difficult isolation of unidentified species.[37]

Scheme 1. Structure of the Triphenylsiloxy Complex of Chromium(II) $[(Ph_3SiO)Cr\cdot(THF)]_2(\mu\text{-}OSiPh_3)_2$ (1) and Its Switching Behavior from Ethylene Polymerization to Nonselective Oligomerization with an Increase in MAO

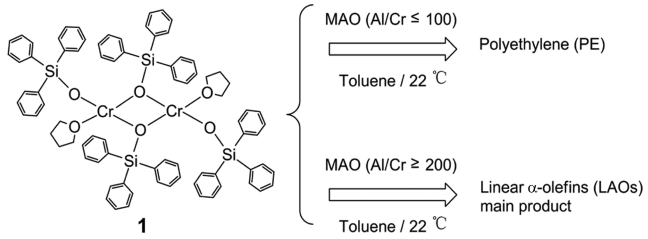

In recent decades, density functional theory (DFT) calculations have been utilized as a powerful tool to identify the active species of many hetero/homogeneous chromium-based catalysts and to elucidate the mechanisms for ethylene polymerization/oligomerization.[38−43] Herein, we attempt to give some deep insight into these unsolved key issues in the **1**/MAO catalyst system through combined experimental and computational approaches. The dependence of catalytic performance on ethylene pressure and structural features of the products were further investigated. Twelve plausible molecular models, **A**−**L**, were proposed as potential active species in the **1**/MAO catalyst system, and then a detailed DFT study on the chain propagation and chain transfer processes was performed over each of these proposed models. As a result, the most plausible active species for ethylene polymerization and ethylene nonselective oligomerization were suggested, and a switching mechanism from ethylene polymerization to ethylene nonselective oligomerization in the **1**/MAO catalyst system was proposed on the basis of the experimental and theoretical results.

2. EXPERIMENTAL AND COMPUTATIONAL METHODS

2.1. Experimental Section. *2.1.1. General Experimental Procedures.* All manipulations with air-sensitive materials were performed with the exclusion of oxygen and moisture in Schlenk-type glassware and a high-vacuum (10^{-6} Torr) line. For storage of materials, a nitrogen-filled Vacuum Atmospheres glovebox with a medium-capacity recirculator (1−2 ppm of O_2) was used. The gases (argon and nitrogen) were purified by passage through a MnO oxygen-removal column and a Davison 4 Å molecular sieve column, and ethylene gas was purified by passage through a Davison 4 Å, 13X molecular sieves and Q-5 reactant catalyst (13 wt % of copper(II) oxide on alumina, Aldrich). Analytically pure solvents were distilled under N_2 from K (tetrahydrofuran), Na/K alloy (toluene), Na (methylcyclohexane). All solvents for vacuum line manipulations were stored in a vacuum over a Na/K alloy. $CrCl_2$ (99.99%, Aldrich), triphenylsilanol (98%, Aldrich), and sodium hydride (95%, Aldrich) were used as received. MAO (Witco) was prepared from a 30% suspension in toluene by evaporation of the solvent at 25 °C/10^{-5} Torr in vacuo. $CDCl_3$ (99.8%, Cambridge Isotope Laboratories) was used as received. Complex **1** was synthesized and characterized as reported in our previous work.[36]

2.1.2. Ethylene Polymerization/Oligomerization. The ethylene polymerization/oligomerization runs of complex **1** were performed in a 100 mL stainless steel reactor equipped

DOI: 10.1021/acscatal.5b00240
ACS Catal. 2015, 5, 3562−3574

Table 1. Results of Ethylene Polymerization/Oligomerization Runs Using Complex 1 with MAO[a]

entry	Al/Cr	amount of PE, (g)	M_w (g mol^{-1})	M_n (g mol^{-1})	activity[c]	amount of oligomers[d] (g)	oligomer distribution[b] (%)						amount of vinyl[e] (mol %)
							C_6	C_8	C_{10}	C_{12}	C_{14}	C_{16}	
1	50	0.39	252 000	31 500	53	0							
2	100	0.23	258 000	33 950	31	0							
3	200	traces[f]			634	4.7	14.3	21.5	23.6	9.8	11.9	6.7	81.5
4	500	traces			701	5.2	11.4	31.2	17.6	16.3	9.9	4.5	77.3
5	1000	traces			756	5.6	10.7	25.2	10.0	21.1	14.0	8.3	74.7
6[g]	100	0.20	235 000	28 300	27								
7[g]	200	traces											
8[h]	50	1.67	185 000	35 580	226	0							
9[h]	100	1.44	223 000	54 390	195	0							
10[h]	200	0.43	141 000	48 620	709	4.8	13.5	16.1	21.8	21.5	14.9	7.2	92.6
11[h]	500	0.31	64 000	29 090	743	5.2	10.1	35.6	11.5	18.9	11.1	6.2	84.2
12[h]	1000	0.34	49 000	21 300	827	5.8	12.3	31.6	16.1	11.0	9.1	9.0	89.1

[a]Standard conditions: T = 22 °C, V = 10 mL, P = 6 atm, catalyst = 10 mg, time = 30 min. [b]By GC, values of C_4 are not given due to volatility, the remainder is C_4 and C_{18+}. [c]Activity (g mmol Cr^{-1} g^{-1}) determined by adding polymerization activity to oligomerization activity. [d]By integration of the NMR olefinic resonances with respect to the Me of the toluene solvent. [e]By integration of the NMR olefinic resonances. [f]Less than 0.05 g. [g]Solvent: methylcyclohexane (10 mL). [h]Results of ethylene polymerization/oligomerization runs using **1**/MAO under 20 atm of ethylene pressure.

with a magnetic stirrer. The reactor was charged with a certain amount of complex **1**, cocatalyst, and solvent (10 mL) inside a glovebox. The reactor was filled with ethylene at a pressure of 6 atm. The pressure was kept constant for 30 min, at which point the temperature was rapidly reduced to 0 °C, and the reaction was quenched by exhausting the unreacted ethylene in a well-ventilated hood, followed by introduction of H_2O/MeOH (10%) to decompose the cocatalyst. Then the organic and aqueous phases were separated from the polymer. The polymer was washed with HCl/MeOH (10%), MeOH, and H_2O and dried at 60 °C for 24 h under reduced pressure before the final mass was weighed. Ratios (or selectivities) of oligomers were obtained by GC by using standard references. The catalytic activity of ethylene nonselective oligomerization was determined by integrating the intensity of the olefinic NMR resonances versus the methyl group of the toluene solvent.

2.1.3. Characterization of the Polymers and the Oligomers. NMR measurements of the oligomers were conducted in $CDCl_3$ and recorded on a Bruker Avance 300 MHz spectrometer. Chemical shifts for ^{1}H NMR were referenced to internal solvent resonances and reported relative to methyl group of toluene. The percentage of vinyl termination was determined by ^{1}H NMR according to the following formula: vinyl content =1 − $[(I_f - 1.5I_a)/2I_f]$, where I_f and I_a are the relative intensities for terminal methyl and terminal vinyl groups of linear oligomers, respectively.[44]

GC analyses were carried out on a Varian 3900 GC. The column had a length of 30 m and internal diameter of 0.25 mm. A gradient oven temperature program, going from 40 °C (for 2 min) to 280 °C at a rate of 10 °C min^{-1} and holding at the final temperature for 3 min, was employed. Linear α-olefins (C_6H_{12}, C_8H_{16}, $C_{10}H_{20}$, $C_{12}H_{24}$, $C_{14}H_{28}$, $C_{16}H_{32}$) and toluene were calibrated by blank GC experiments. Molecular weights of polymer were determined by the GPC method on a Waters-Alliance 2000 instrument using 1,2,4-trichlorobenzene as a mobile phase at 160 °C and referenced to polystyrene standards. FT-IR spectra of thin films on KBr plates were recorded on a FT-IR Avatar 380 spectrometer. Melting crystallization behavior of the polymers was examined using a Thermal Analysis Q200 differential scanning calorimeter. Three runs (heating−cooling−heating) at a rate of 10 °C min^{-1} in the range 30−180 °C were performed for each sample of polymer. The second heating exothermal peak temperature was taken as a melting point.

2.2. Computational Details. All DFT calculations, including geometry optimizations, frequency calculations, and full intrinsic reaction coordinate (IRC) calculations, were performed in Gaussian09.[45] Geometry optimizations were performed without any symmetry constraint using the B3LYP[46−48] functional in combination with the triple-ζ basis set with the effective core potential of Hay and Wadt (LANL2TZ(f)) for Cr and the full electron Pople's triple-ζ basis set 6-311G(d,p) for all other atoms. Throughout, we have employed harmonic vibrational frequency calculations to confirm that structures have been properly optimized. Each transition state was further verified by a full IRC calculation,[49] which showed a direct connection between the corresponding reactant and the product. Solvation effects were incorporated into the geometry optimizations by using a polarizable continuum model (PCM),[50,51] portraying toluene as the model solvent. The dispersion corrections were calculated using the DFT-D3 (zero-damping) code developed by Grimme and co-workers recently.[52−55] Energies reported refer to Gibbs free energy corrections to the total electronic energies at 295 K and 20 atm. Geometry optimization of each structure in each model was conducted under all possible spin states to identify the ground spin states as summarized in Table S1 in the Supporting Information. The results indicated that the quartet for Cr(III), the quintet for Cr(II), and sextet for Cr(I) were identified as the ground spin states for all the plausible molecular models. In this work, the Cr-alkyls for ethylene insertion and β-hydrogen transfer processes contained a β-agostic structure (X_β), which were proven to be more stable chain orientations than γ-agostic structure (X_γ).[56,57]

3. RESULTS AND DISCUSSION

3.1. Ethylene Polymerization/Oligomerization under Different Conditions. In our previous report, the **1**/MAO catalyst system presented a switching behavior from ethylene polymerization (Al/Cr $\leqslant$ 100) to ethylene nonselective oligomerization (Al/Cr $\geqslant$ 200) with increasing Al/Cr molar ratio under 20 atm of ethylene pressure.[36] To elucidate the

DOI: 10.1021/acscatal.5b00240
ACS Catal. 2015, 5, 3562−3574

influence of ethylene pressure on catalytic performance, the ethylene polymerization/oligomerization runs were carried out under 6 atm of ethylene pressure in this work. A summary of the ethylene polymerization/oligomerization results is given in Table 1. A very similar switching behavior from ethylene polymerization (Al/Cr $\leq$ 100) to ethylene nonselective oligomerization (Al/Cr $\geq$ 200) was observed under 6 atm of ethylene pressure. It is noteworthy that the oligomerization activities under 6 atm (entries 3−5) are very similar to those under 20 atm (entries 10−12). Thereby, we inferred that the oligomerization activities were almost independent of ethylene pressure in the **1**/MAO catalyst system. On the basis of this experimental result, we can suggest that the ethylene nonselective oligomerization could most probably proceed through the Cossee−Arlman mechanism rather than the metallacycle mechanism, which generally was proposed for ethylene selective oligomerization catalysts with a second-order dependence of catalyst activity on ethylene pressure.[58,59] The following DFT studies of chain propagation process over all plausible molecular models of active sites will be performed on the basis of Cossee−Arlman mechanism. In addition, only solid polyethylene (entry 6) but no liquid oligomers (entry 7) was obtained when the solvent was changed from toluene to methylcyclohexane, and these results implied that toluene might play an important role for generation of the ethylene nonselective oligomerization active species in the **1**/MAO catalyst system. Hence, in the following DFT studies, active species models coordinated by toluene molecules will be considered.

^{1}H NMR results revealed the oligomerization products with high contents of terminal vinyl groups (entries 10−12), and these results indicated the main oligomerization products were linear α-olefins (LAOs).[36] In addition, GC results showed that oligomerization products were mainly even-numbered LAOs (C_6−C_{16}). Therefore, β-hydrogen transfer was confirmed as the major chain transfer mechanism for ethylene nonselective oligomerization.[60−63] Moreover, the FT-IR spectrum of polyethylene product (Figure 1) showed the obvious vibrations associated with terminal vinyl groups (ν = 908 and 991 cm^{-1}),[57] which also indicated that β-hydrogen transfer was the major chain transfer mechanism for ethylene polymerization.[52−55] However, β-hydrogen transfer can occur either (i) to the coordinating ethylene monomer (BHT) or (ii) to the chromium center (β-hydrogen elimination, BHE). In the first case, the M_w of the obtained polymer would be independent of ethylene pressure. Conversely, in the latter case, the M_w of the obtained polymer would be dependent upon the ethylene concentration.[10,64]It can be seen from Table 1 (entries 1−2, and 8−9) that the M_w of the PE slightly decreased with an ethylene pressure change from 6 to 20 atm at the low Al/Cr molar ratios. Thereby, from the experimental results, BHE (transfer to the chromium center) would be a major chain transfer mechanism rather than BHT (transfer to the coordinating ethylene). In the next section, further DFT calculations also indicate that BHE is the major chain termination mechanism in the present **1**/MAO catalyst system because of the failure to locate the transition state of β-hydrogen transferred to the coordinating ethylene.

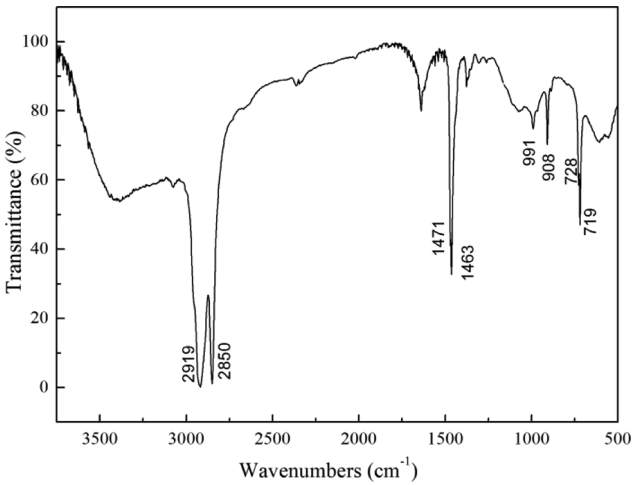

Figure 1. Typical FT-IR spectrum of solid PE produced with **1**/MAO (Al/Cr = 500) under 20 atm of ethylene pressure.

3.2. Molecular Modeling of Active Species and Their Switching Mechanism. In recent decades, molecular modeling, especially using the DFT method, has played an increasingly important role in deeper mechanistic understanding of the transition-metal-based polymerization catalysts. One of the main advantages of theoretical modeling is that we can separate all the mechanistic steps, including detailed elementary reactions, that are difficult or inaccessible for experimental techniques. As for searching the homogeneous chromium catalyst systems for ethylene polymerization or oligomerization, obviously, isolating active intermediates from the catalyst systems would be the best way to get insight into the reaction mechanism and oxidation state of the metal center. However, isolable active species are relatively rare for many reactions, and the chromium species experimentally observed may not be relevant to catalysis, which makes it very difficult to establish the direct link between the structures of active site and catalytic activity of the catalyst. For this reason, DFT calculations can provide us much valuable information at a molecular and atomic level for mechanistic understanding of the catalytic cycle and for recognizing the most probable active species.

3.2.1. Proposed Models of Active Species and Catalytic Cycle. In our previous work, the activation of complex **1** $[(Ph_3SiO)Cr\cdot(THF)]_2(\mu\text{-}OSiPh_3)_2$ with MAO was investigated by ESR and ^{29}Si NMR spectroscopy.[36] On the basis of the results, the Cr−methyl (Cr−Me) species were proposed to be generated by alkylation reaction. During the activation, a Cr−C bond was generated by transferring the methyl group from MAO to the chromium center, and the Ph_3SiO− group could be transferred from the chromium center to the aluminum of MAO. Similar ligand exchange has been suggested in MAO activation of halide metallocene complexes such as Cp_2ZrCl_2[65,66] and $Cp_2Ti(CH_3)Cl$.[67,68] In view of the binuclear Cr(II) complex **1** activated by MAO, it is rational to consider Cr(II) and Cr(I) as the potential Cr oxidation states of the active species; however, Cr(III) cannot be fully excluded as the potential valence state of the active species on the basis of the limited experimental results. As mentioned above, the alkyl aluminum activator may indirectly induce reoxidation of Cr(II) toward the Cr(III) catalyst precursor through a disproportionation reaction, as reported by Gambarotta and Duchateau et al.[35] This proposal implies that a chromium species with a valence state lower than 2 must be generated at the same time, and it could be a driving force for this disproportionation reaction that 0- and monovalent chromium−arene complexes[69,70] have well-established stability. In fact, the ESR

DOI: 10.1021/acscatal.5b00240
ACS Catal. 2015, 5, 3562−3574

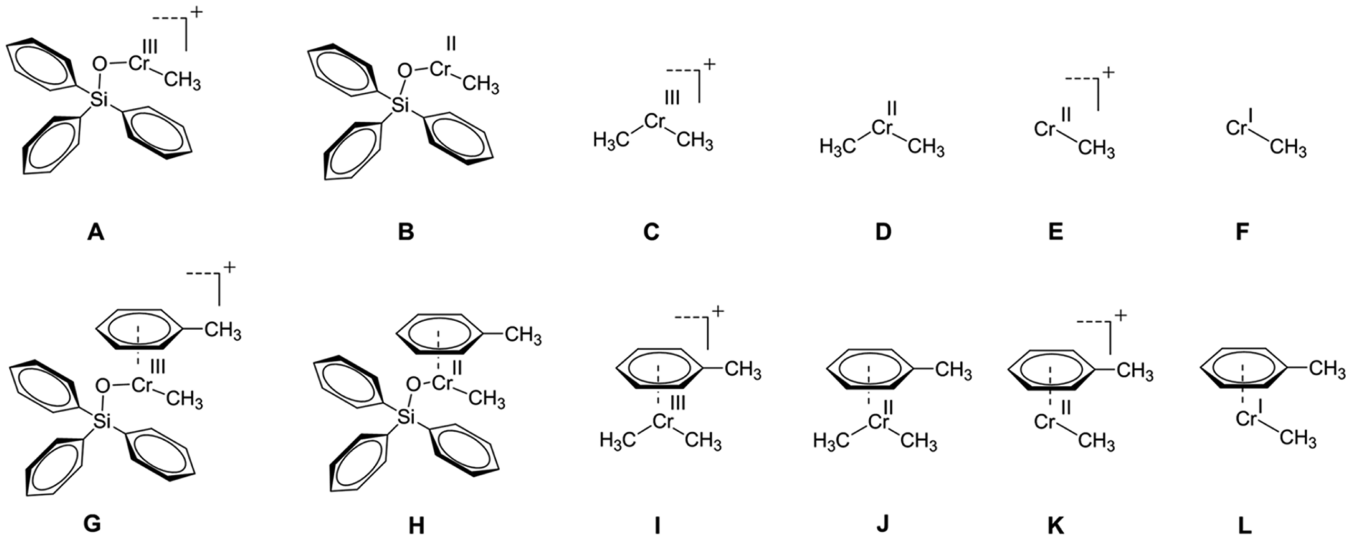

Figure 2. Molecular models used in this work. (**A**, $[(Ph_3SiO)Cr^{III}Me]^+$; **B**, $(Ph_3SiO)Cr^{II}Me$; **C**, $[Cr^{III}Me_2]^+$; **D**, $Cr^{II}Me_2$; **E**, $[Cr^{II}Me]^+$; **F**, $Cr^{I}Me$; **G**, $[(Ph_3SiO)Cr^{III}Me]^+$/toluene; **H**, $(Ph_3SiO)Cr^{II}Me$/toluene; **I**, $[Cr^{III}Me_2]^+$/toluene; **J**, $Cr^{II}Me_2$/toluene; **K**, $[Cr^{II}Me]^+$/toluene; **L**, $Cr^{I}Me$/toluene).

Scheme 2. Proposed Catalytic Pathways for the 1/MAO Catalyst System in This Work[a]

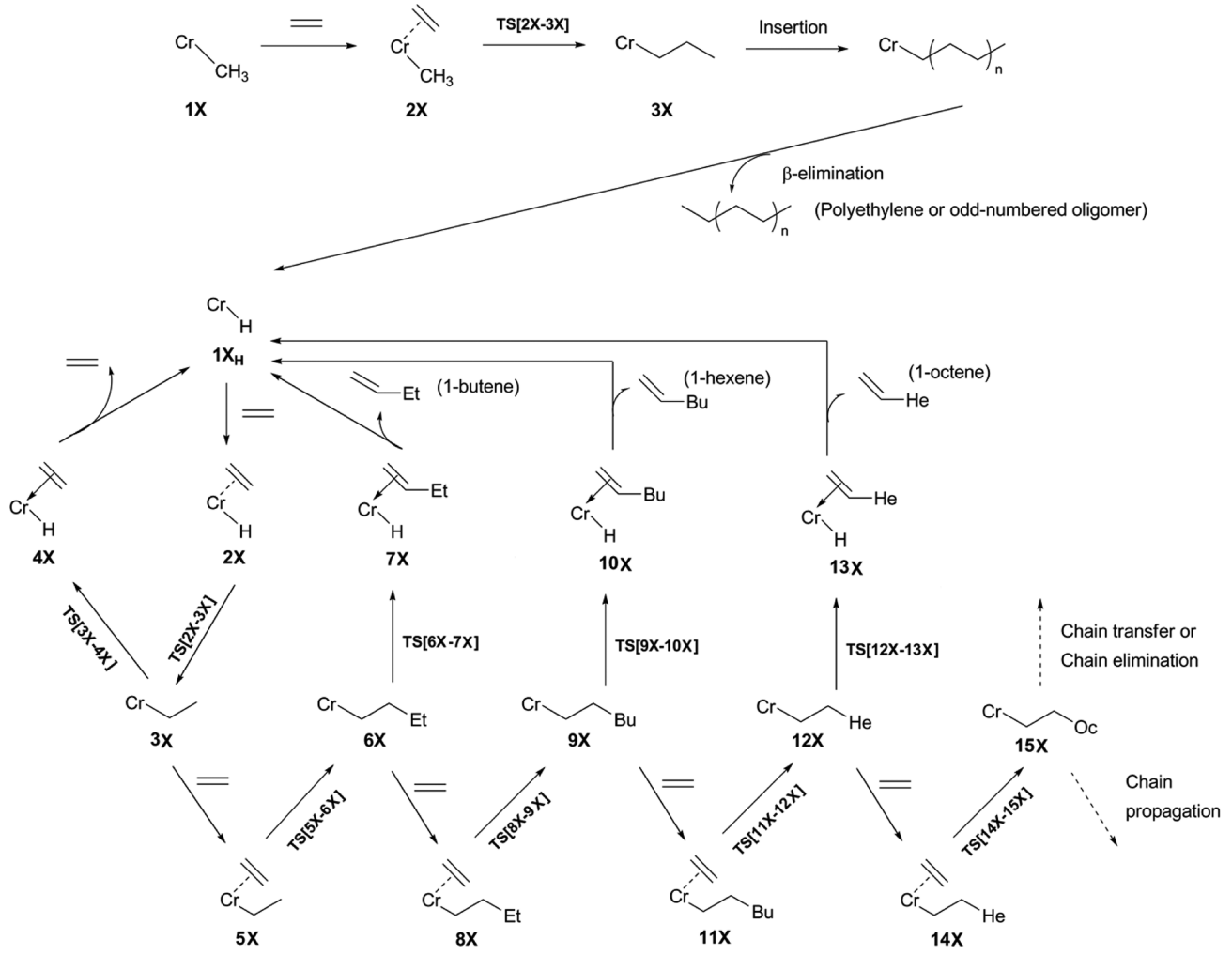

[a]**X** signifies the labeling of 12 plausible molecular models (**A**–**L**). Et, ethyl group; Bu, butyl group; He, hexyl group; Oc, octyl group.

spectrum of complex **1** activated by MAO (Al/Cr =100) in toluene at 290 K identified the formation of an inactive cationic monovalent $[Cr(I)(\eta^6\text{-arene})_2]^+$ sandwich complex. Therefore, herein, Cr(III) complexes are also considered as the potential active species in the following DFT calculations. Consequently, 12 plausible molecular models, **A**–**L**, bearing Cr(I)–Me,

DOI: 10.1021/acscatal.5b00240
ACS Catal. 2015, 5, 3562–3574

Cr(II)−Me and Cr(III)−Me species are proposed as the potential active species for ethylene polymerization/oligomerization, as shown in Figure 2. Among the 12 models, models **A**−**F** are the plausible active species without considering the coordination of the solvent molecule (toluene), and models **G**−**L** are the corresponding molecular models with the consideration of toluene coordination. These 12 molecular models (**A**−**L**) of active species in the **1**/MAO catalyst system are further studied for the chain propagation process.

In this work, the catalytic cycle is designated on the basis of the Cossee−Arlman mechanism, which has been well established for ethylene polymerization[13,14] (Scheme 2). It has been discussed in the Experimental section that the ethylene nonselective oligomerization activities are almost independent of ethylene pressure in the **1**/MAO catalytic system, which is not completely consistent with the metallacycle mechanism for selective trimerization catalysts with a second-order dependence of catalyst activity on ethylene pressure.[58,59]

As illustrated in Scheme 2, **X** signifies the labeling of 12 plausible molecular models (**X** = **A**−**L**), including six neutral and six cationic models for the active species of the **1**/MAO catalyst system. In general, the starting structure compound **1X** possesses one ethylene molecule coordination to the chromium center, resulting in the formation of the π complex **2X**. The double bond of ethylene is debilitated by the charge-transfer process of donation and back-donation interactions between ethylene and the chromium center. Therefore, in the transition state **TS**[**2X**−**3X**], a four-membered ring is formed by the Cr, C_α, and two C atoms from the incoming ethylene molecule. Finally, the chromium bonds to the nearest ethylene C atom, and the other ethylene C atom bonds to the C_α with the formation of **3X**. This process is one insertion of an ethyl unit ($-CH_2-CH_2-$) in the growing polymer chain and is repeated until a termination reaction occurs. It is noted that every attempt to locate the transition state of β-hydrogen transferred to the coordinated ethylene molecule failed, which could be attributed to the steric effect. Therefore, combined with the experimental results, a β-hydrogen being transferred to chromium center is considered to be the major chain transfer mechanism in the following DFT caculations, and the newly generated active species of Cr−H are ready for the following reactions, which are referred to as $\mathbf{1X_H}$ in Scheme 2. Ethylene monomers continue to react with $\mathbf{1X_H}$ to form the polymer chain or to generate oligomer products including a series of even-number α-olefins.

3.2.2. Initial Model Screening through the First Ethylene Insertion. Detailed analyses of energetic and geometric aspects of the step for the models **A**−**L** are presented in this section. Because the ethylene insertion is crucial for the polymerization process, we compared the ethylene coordination energy and the barrier for ethylene insertion into the Cr−Me bond over the 12 active species models **A**−**L**. Relative Gibbs free energies for the stationary points of ethylene insertion for models **A**−**L** are given in Table 2. Both models **G**, [(η^4-toluene)Cr^{III}(Ph_3SiO)-Me]$^+$, and **H**, (η^2-toluene)Cr^{II}(Ph_3SiO)Me, cannot be coordinated by ethylene molecules to generate π complexes; the ethylene molecule is invariably expelled from the coordination sphere of chromium during the geometry optimizations. The geometrical features of the stationary points and relative Gibbs free energies along the reaction path of ethylene insertion are presented in Figure 3 for model **A** [(Ph_3SiO)Cr^{III}Me]$^+$.

Table 2. Gibbs Free Energies of Ethylene Insertion into the Cr−Methyl Bond via Cossee−Arlman Mechanism for Models A−L[a]

	energy relative to separated reactants			
model	ΔG_{295}(**2X**)	ΔG_{295} (**TS**[**2X**−**3X**])	ΔG_{295}(**3X**)	insertion barriers, $\Delta G^{\ddagger}_{295}$
A	−1.8	13.5	−7.0	15.3
B	0.4	22.1	−5.5	22.1
C	−4.7	10.2	−11.2	14.9
D	4.6	19.4	−6.3	19.4
E	−5.6	9.5	−7.5	15.1
F	−3.5	36.8	−7.5	40.3
G				
H				
I	−4.2	6.5	−9.2	10.7
J	13.4	22.8	−4.6	22.8
K	−4.3	8.7	−7.9	13.0
L	−1.3	30.4	−7.9	31.7

[a]Gibbs free energies are in kcal/mol and relative to **1X**, and coordination energy should be added to the energy barrier if the free energy of the π complex is higher than the reactant and free ethylene.

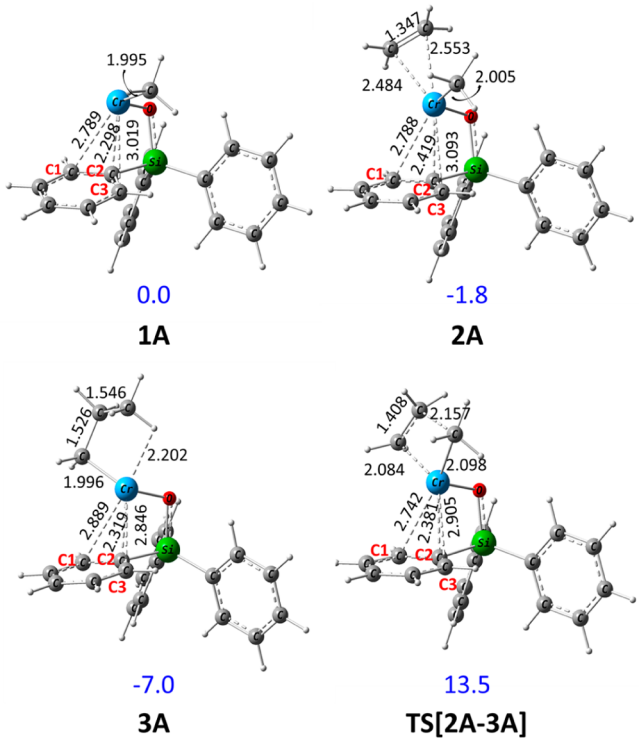

Figure 3. Gibbs free energies (kcal/mol, relative to **1A**) and geometries of stationary points of ethylene insertion for [(Ph_3SiO)-Cr^{III}Me]$^+$ (**A**) as optimized with the DFT approach. Bond distances are in angstroms.

The active species model **A** [(Ph_3SiO)Cr^{III}Me]$^+$ consists of one central chromium atom bonded with a methyl group and a triphenylsiloxy group in which the chromium is η^1-coordinated by one phenyl group, which results in a more stabilized geometry by lowering the positive charge density of the central cationic chromium. As shown in Figure 3, for the initial ethylene coordination and insertion steps, the distances between the central Cr and C2 (the carbon atom of the η^1-coordinated phenyl group) are from 2.298 to 2.419 Å, which

DOI: 10.1021/acscatal.5b00240
ACS Catal. 2015, 5, 3562−3574

indicates a strong interaction between Cr and C2. In contrast, the interaction between the central Cr and C1, C3 are relatively weak, with distances from 2.742 to 3.093 Å. The insertion step is initiated by an ethylene monomer approaching the model **1A**, leading to the formation of a π-complex **2A**.

The coordination of ethylene in **2A** leads to two relatively long Cr−C bonds of 2.484 and 2.553 Å and a slight elongation of the C═C double bond (ethylene) by 0.019−1.347 Å. The Cr−Me bond has stretched from 1.995 to 2.005 Å in **2A**. The total π-complexation energy amounts to −1.8 kcal/mol, compared to **1A** and free ethylene, indicating that the ethylene coodination to model **1A** is an exoergic process. The insertion process proceeds after the formation of the π complex **2A** to give 3**A** through the transition state **TS**[**2A**−**3A**]. The geometry for **TS**[**2A**−**3A**] has been determined by the standard algorithm of transition state optimization and confirmed by a full IRC calculation. The Cr−Me bond is elongated from 1.995 Å in the reactant **1A** to 2.098 Å in **TS**[**2A**−**3A**], and a partial C−C bond of 2.157 Å is formed in **TS**[**2A**−**3A**]. Thus, the structure **TS**[**2A**−**3A**] is a typical four-center transition state consisting of ethylene, the methyl group, and chromium, consistent with the classic Cossee-Alrman mechanism.[14]

The barrier associated with **TS**[**2A**−**3A**] is calculated to be 15.3 kcal/mol relative to the π-complex **2A**. The kinetic insertion product formed from the transition state **TS**[**2A**−**3A**] is the γ-agostic propyl complex **3A** which is 5.2 kcal/mol more stable than the π complex **2A**. In fact, when model **A**, $[Cr^{III}(Ph_3SiO)Me]^+$, is coordinated by one molecular toluene to generate model **G**, $[(\eta^4\text{-toluene})Cr^{III}(Ph_3SiO)Me]^+$, we can get not only model **G** but also model **G**′, as shown in Figure S1 in the Supporting Information. For model **G**, the chromium center is η^4-coordinated by toluene in which one hydroden atom of the toluene's methyl is hydrogen-bonded to the oxygen atom in the ligand Ph_3SiO− group. On the other hand, for model **G**′, the chromium center is only η^4-coordinated by toluene, in which the methyl of toluene is in the opposite position of the oxygen atom in the ligand Ph_3SiO− group. The relative Gibbs free energies of model **G**′ and **A** is −0.01 kcal/mol, which indicates that the interaction between the benzene ring of tolune and chromium is very weak, and model **G** is slightly, but not strongly, more stable than model **A** (−2.42 kcal/mol). Therefore, model **A** can be possibly existing in this **1**/MAO catalyst system, especially under high ethylene pressure.

The geometrical features of the stationary points along the reaction path of ethylene insertion for the divalent neutral model **B**, $(Ph_3SiO)Cr^{II}Me$, are found to be quite different from its isomer model, **A**. No internal phenyl group in the triphenylsiloxy group could be coordinated to the central chromium atom, which should be attributed to the different chromium oxidation states and electric charge density. The coordination of one ethylene yielded **2B** with an endoergic effect of 0.4 kcal/mol, and subsequent insertion to the Cr−Me bond has a higher energy barrier of 21.7 kcal/mol. Therefore, the total energy barrier of initial ethylene insertion for model **B** is 22.1 kcal/mol, which is 6.8 kcal/mol higher than that of model **A**. As for cationic dialkyl-Cr(III) species model **C**, $[Cr^{III}Me_2]^+$, and **I**, $[(\eta^6\text{-toluene})Cr^{III}Me_2]^+$, the π complexes **2C** and **2I** are 4.7 and 4.2 kcal/mol more stable, respectively, than infinitely separated reactants (see Table 2). In contrast, the coordination of one ethylene over the neutral dialkyl-Cr(II) species models **D**, $Cr^{II}Me_2$, and **J**, $(\eta^6\text{-toluene})Cr^{II}Me_2$, shows an apparent endoergic effect of 4.6 and 13.4 kcal/mol, respectively, so the two related π complexes **2D** and **2J** are quite unstable. Meanwhile, both models **D** and **J** present much higher energy barriers (19.4 and 22.8 kcal/mol, respectively) for ethylene insertion than cationic dialkyl-Cr(III) species model **C**, $[Cr^{III}Me_2]^+$, and **I**, $[(\eta^6\text{-toluene})Cr^{III}Me_2]^+$ (14.9 and 10.7 kcal/mol, respectively), which is in agreement with other theoretical results.[71,72]

With the same trend, cationic monoalkyl-Cr(II) species models **E**, $[Cr^{II}Me]^+$, and **K**, $[(\eta^6\text{-toluene})Cr^{II}Me]^+$, generate more stable π complexes than related neutral monoalkyl-Cr(I) models **F**, $Cr^{I}Me$, and **L**, $(\eta^2\text{-toluene})Cr^{I}Me$. The optimized geometry of model **L** shows a displacement of the MeCr fragment toward a pseudo-η^2 coordination mode, which is in agreement with the theoretical study on monomeric MeCr−C_6H_6 species (see Figure 4).[73] In addition, the insertion process

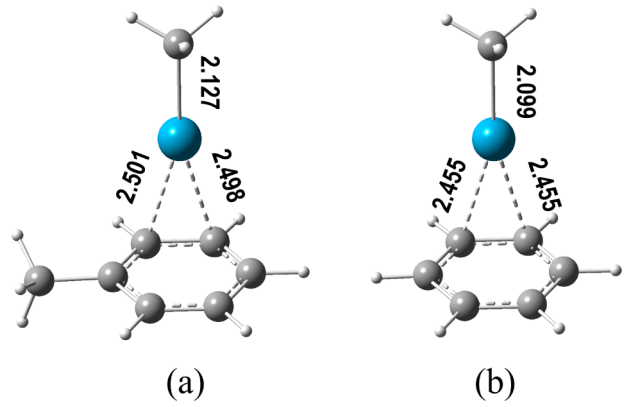

Figure 4. DFT-optimized structures of the MeCr(I)−toluene model **L** (a) and the MeCr(I)−benzene model (b).

of models **F** and **L** are prohibited by showing significantly higher energy barriers of 30−40 kcal/mol than that of models **E** and **K** (15.1 and 13.0 kcal/mol, respectively); thus, these neutral monoalkyl-Cr(I) models **F** and **L** are not favored for the insertion reactions of ethylene. Generally, the Cr(I) species is considered to be stabilized by aromatic compounds such as toluene, with which it generates catalytically inactive η^6-arene compouds.[73−75] Another six possible neutral Cr(III) models were also investigated and are discussed in great detail in the Supporting Information (Section S1, Figure S2, and Table S2); they showed unstable π complex and higher ethylene insertion energies.

Consequently, after the initial model screening through the insertion of the first ethylene monomer, active species models **A** $[(Ph_3SiO)Cr^{III}Me]^+$, **C** $[Cr^{III}Me_2]^+$, **E** $[Cr^{II}Me]^+$, **I** $[(\eta^6\text{-toluene})Cr^{III}Me_2]^+$, and **K** $[(\eta^6\text{-toluene})Cr^{II}Me]^+$ with more stable π complexes and lower ethylene insertion energy barriers are proposed to be the most plausible molecular models of active species for ethylene polymerization/oligomerization in the **1**/MAO catalyst system. In the next subsection, DFT studies are applied to give more information on the competition between chain propagation and chain transfer over these five models through a secondary model screening to elucidate which model is responsible for the ethylene polymerization or ethylene nonselective oligomerization.

3.2.2. Secondary Model Screening through Successive Chain Propagation/Transfer Reactions. It is mentioned in the Experimental section that the obtained oligomers are identified as even-numbered LAOs, which cannot be produced by ethylene insertion and β-hydrogen transfer to chromium center

DOI: 10.1021/acscatal.5b00240
ACS Catal. 2015, 5, 3562−3574

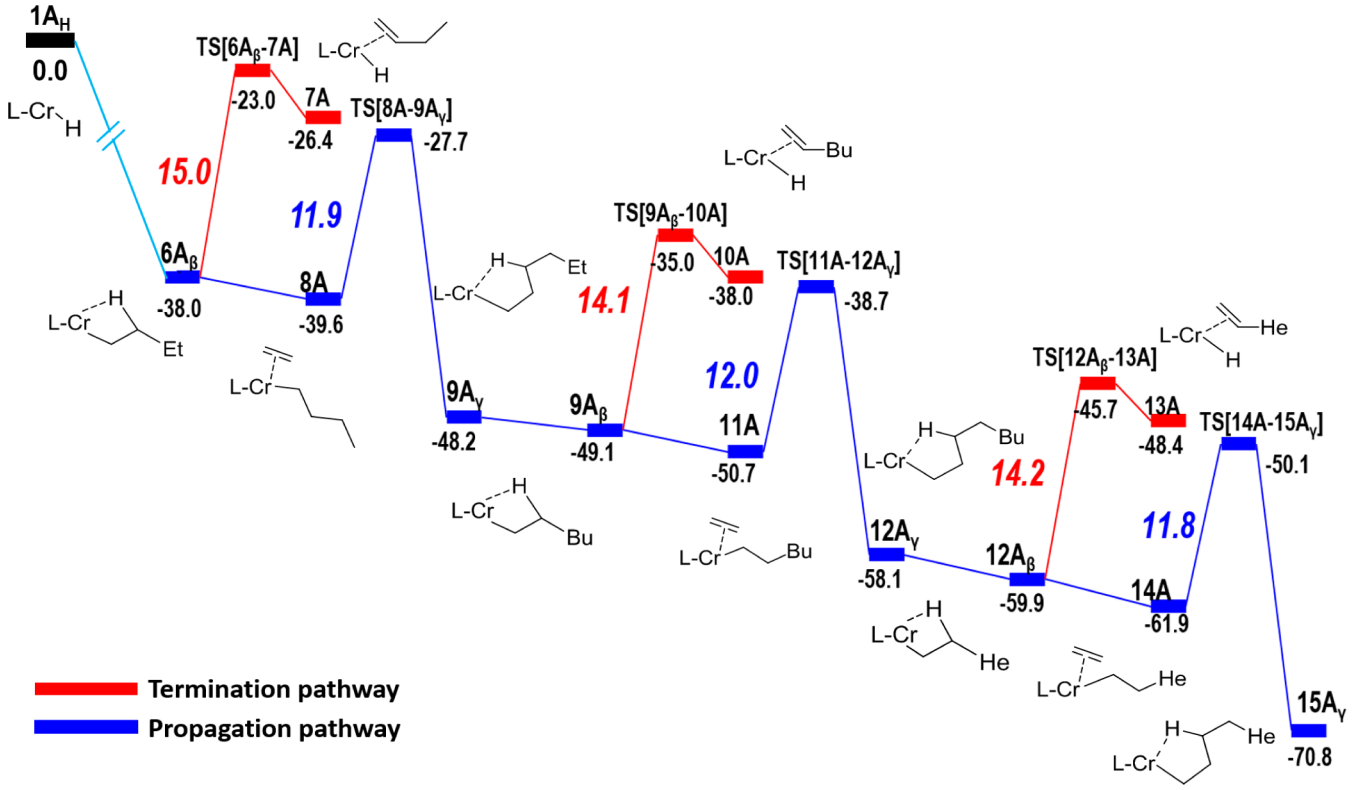

Figure 5. Gibbs free-energy profile (kcal/mol, relative to $\mathbf{1A_H}$ plus the corresponding number of free ethylene molecules) for propagation (blue) and termination (chain transfer, red) pathways for ethylene polymerization/oligomerization starting from $\mathbf{6A_\beta}$. L, Ph_3SiO- group; Et, ethyl group; Bu, butyl group; He, hexyl group. Energetic barriers are indicated in italics.

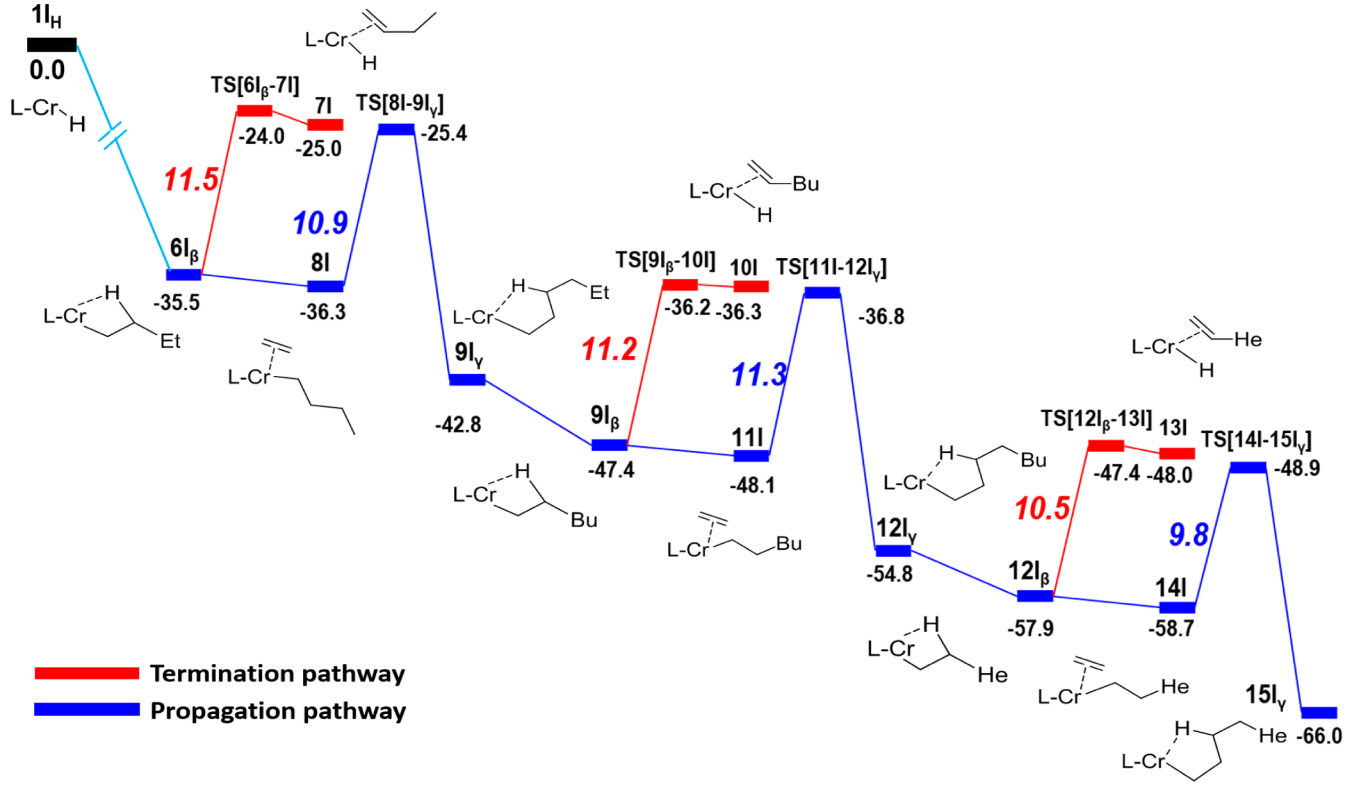

Figure 6. Gibbs free-energy profile (kcal/mol, relative to $\mathbf{1I_H}$ plus the corresponding number of free ethylene molecules) for propagation (blue) and termination (chain transfer, red) pathways for ethylene polymerization/oligomerization starting from $\mathbf{6I_\beta}$. L, toluene; Et, ethyl group; Bu, butyl group; He, hexyl group. Energetic barriers are indicated in italics.

DOI: 10.1021/acscatal.5b00240
ACS Catal. 2015, 5, 3562−3574

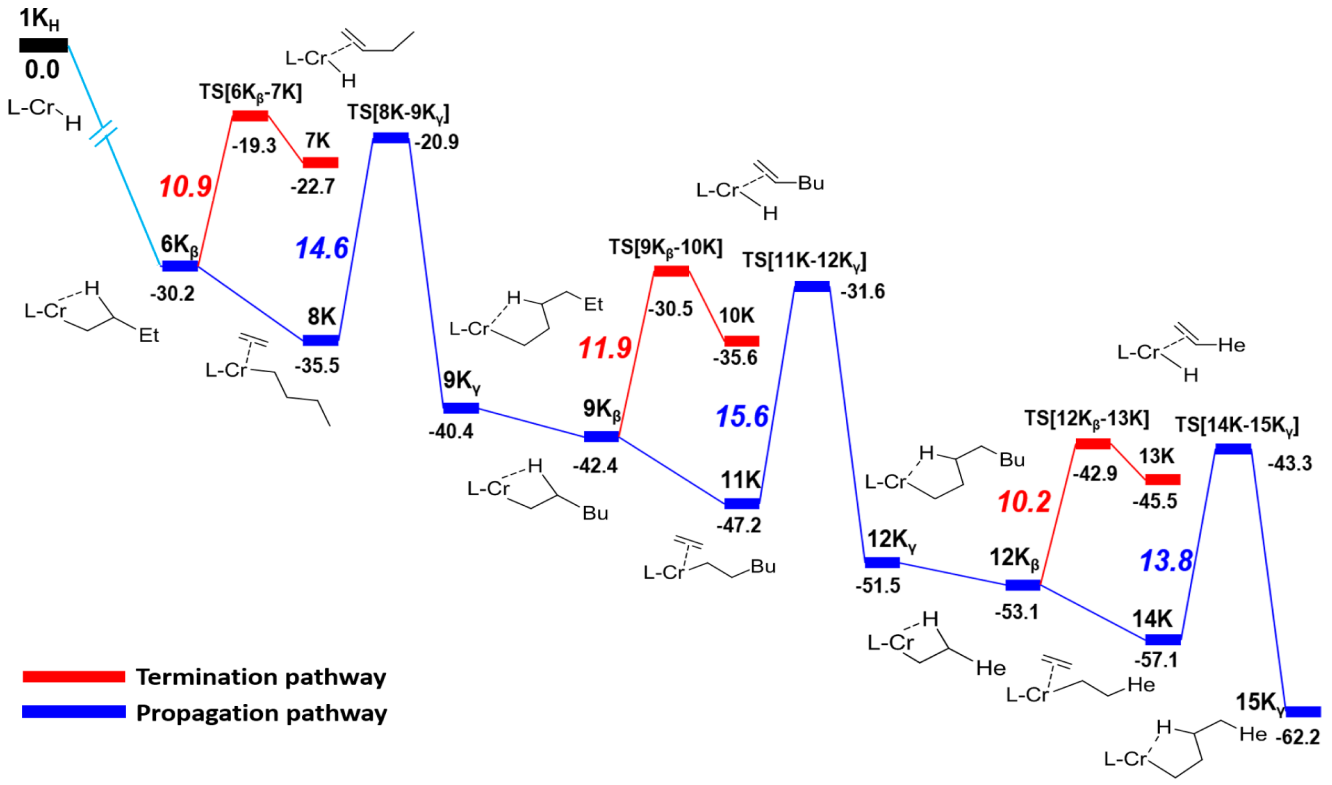

Figure 7. Gibbs free-energy profile (kcal/mol, relative to $\mathbf{1K_H}$ plus the corresponding number of free ethylene molecules) for propagation (blue) and termination (chain transfer, red) pathways for ethylene polymerization/oligomerization starting from $\mathbf{6K_\beta}$. L, toluene; Et, ethyl group; Bu, butyl group; He, hexyl group. Energetic barriers are indicated in italics.

Table 3. Energy Barriers (kcal/mol) of Ethylene Insertion (I) and α-Olefin Liberation via β-H Transfer to Cr Center (T) and the Differences between the two Energy Barriers for 3X−12X (X = A, C, E, I, and K)

	A			C			E			I			K		
	I^a	T^b	$\Delta(I-T)$	I^a	T^b	$\Delta(I-T)$	I^a	T^b	$\Delta(I-T)$	I^a	T^b	$\Delta(I-T)$	I^a	T^b	$\Delta(I-T)$
3X	13.3	17.8	−4.5	11.8	16.6	-4.8	14.8	15.6	−0.8	10.4	14.5	−4.1	13.3	15.4	−2.1
6X$_\beta$	11.9	15.0	−3.1	10.9	10.4	+0.5	13.5	11.1	+2.4	10.9	11.5	−0.6	14.6	10.9	+3.7
9X$_\beta$	12.0	14.1	−2.1	11.2	10.9	+0.3	14.1	11.4	+2.7	11.3	11.2	+0.1	15.6	11.9	+3.7
12X$_\beta$	11.8	14.2	−2.4	9.7	11.4	−1.7	13.8	10.8	+3.0	9.8	10.5	−0.7	13.8	10.2	+3.6

[a]Energy barriers of **TS[5X−6X]** for **3X**, **TS[8X−9X]** for **6X$_\beta$**, **TS[11X−12X]** for **9X$_\beta$**, and **TS[14X−15X]** for **12X$_\beta$**. [b]Energy barriers of **TS[3X−4X]** for **3X**, **TS[6X−7X]** for **6X$_\beta$**, **TS[9X−10X]** for **9X$_\beta$**, and **TS[12X−13X]** for **12X$_\beta$**.

processes based on Cr−Me species. In fact, the first molecule product (either an odd-numbered oligomer molecule or polyethylene) is produced via ethylene insertion and β-hydrogen elimination processes over the Cr−Me species, accompanied by the formation of a new Cr−H species, $\mathbf{1X_H}$. The model $\mathbf{1X_H}$ is very active for ethylene insertion to generate **3X** (Cr−ethyl, X = **A**, **C**, **E**, **K**, or **I**), and the energy barriers of ethylene insertion are no more than 2.6 kcal/mol (see Table S3, Supporting Information). In the following section, four consecutive ethylene insertions (chain propagation) and the corresponding β-hydrogen elimination (chain transfer) processes over these five models are investigated to differentiate polymerization active species from oligomerization active species, as shown in Scheme 2.

Calculation results of models **A** $[(Ph_3SiO)Cr^{III}Me]^+$, **I** $[(\eta^6\text{-toluene})Cr^{III}Me_2]^+$, and **K** $[(\eta^6\text{-toluene})Cr^{II}Me]^+$ in terms of their free-energy diagrams along the reaction paths are shown in Figures 5, 6, and 7, respectively. As for the chain propagation process, the geometrical features of the stationary points along the reaction path of ethylene insertion over model $\mathbf{1A_H}$ are found to be very similar to the structures shown in Figure 3. After the initial ethylene insertion into the Cr−H bond, four consecutive ethylene insertions present a similar energy barrier, 11.8−13.3 kcal/mol (Figure 5). In terms of the process for β-hydrogen transfer to the chromium center, the energy barriers are 17.8, 15.0, 14.1, and 14.2 kcal/mol, producing α-olefins from the four intermediates **3A**, **6A$_\beta$**, **9A$_\beta$**, and **12A$_\beta$**, respectively, which are constantly higher than those of the ethylene insertion process in their corresponding pathways. As listed in Table 3, the activation energy differences between β-hydrogen elimination and ethylene propagation are more than 2.0 kcal/mol. Since M_w should be proportional to the ratio of the propagation rate/chain transfer rate,[37,76] these results indicate that model **A** appears to be a rational catalyst model for ethylene polymerization rather than for ethylene oligomerization.

Compared with model **A**, $[(Ph_3SiO)Cr^{III}Me]^+$, cationic dialkyl-Cr(III) species models **C**, $[Cr^{III}Me_2]^+$, and **I**, $[(\eta^6\text{-toluene})Cr^{III}Me_2]^+$ (Figure 6), present (2−4 kcal/mol) lower energy barriers for both the process of ethylene propagation

DOI: 10.1021/acscatal.5b00240
ACS Catal. 2015, 5, 3562−3574

and β-hydrogen elimination. After the second ethylene insertion into the Cr−C bond over models **C** and **I**, the energy differences between β-hydrogen elimination and ethylene propagation are so small (−1.7 to +0.5 kcal/mol) that the propagation rate and chain transfer rate are almost considered to be the same (See Table 3). It is to be noted, however, that energy barriers between the α-olefin products and the related transition states of the chain transfer process are no more than 1 kcal/mol, indicating that the chain transfer process is quite thermodynamically disfavored. In addition, all intermediates and transition states of the cationic active species model **I** along the reaction path are apparently more stable (over 9.7 kcal/mol) than that of the simple and naked dialkyl-Cr(III) model **C** $[Cr^{III}Me_2]^+$ in the toluene solvent (Table S4, Supporting Information). With regard to these results, the cationic active species model **I** rather than model **C** appears to be another possible active species model for ethylene polymerization.

For the cationic monoalkyl-Cr(II) species models **E**, $[Cr^{II}Me]^+$, and **K**, $[(\eta^6\text{-toluene})Cr^{II}Me]^+$, calculated free energy diagrams are quite different from that of the cationic Cr(III) model **C** $[Cr^{III}Me_2]^+$ and **I** $[(\eta^6\text{-toluene})Cr^{III}Me_2]^+$. As observed for model **K** in Figure 7, the barrier of the second ethylene insertion into the Cr−C bond is 2.1 kcal/mol lower than that of β-hydrogen elimination process from the intermediate **3K** (13.3 and 15.4 kcal/mol, respectively). However, the models **6K**$_\beta$, **9K**$_\beta$, and **12K**$_\beta$ exhibit much lower energy barriers for the β-hydrogen elimination process (10.2−11.9 kcal/mol) than that for the ethylene insertion process (13.8−15.6 kcal/mol). The energetic differences between chain propagation and chain transfer are up to 3.6 kcal/mol. The geometrical feature of the transition state and energy barriers for the β-hydrogen elimination process shown in Figure S3 (Supporting Information) are consistent with the theoretical studies (9.7−14.6 kcal/mol) of ansa-bis(Cp)Zr catalyst by Talarico and Cavallo et al.[77] Therefore, we considered that model **K** could generate LAOs 1-butene, 1-hexene, 1-octene, and beyond by ethylene insertion and β-hydrogen elimination processes as a reasonable ethylene nonselective oligomerization active species model. No 1-butene is detected by GC analysis, which may be attributed to its high volatility.

The naked model **E**, $[Cr^{II}Me]^+$, without coordination by toluene exhibited behavior similar to that of model **K**, $[(\eta^6\text{-toluene})Cr^{II}Me]^+$; however, the Gibbs free energies of all intermediates and transition states of the cationic model **K** decreased by more than 9.9 kcal/mol after being coordinated by one toluene molecule than that of model **E** (Table S5, Supporting Information), which suggested that the η^6-toluene-coordinated model **K** is much more stable in the toluene solvent. Moreover, the experimental results showed that no liquid oligomers (entry 7, Table 1) were obtained using methylcyclohexane instead of toluene as the solvent and implied that toluene played a key role for generation of the ethylene oligomerization active species. Thus, combined with experimental and DFT results, model **K** is proven to be a more promising active species model for the ethylene nonselective oligomerization than model **E**.

In addition, it was mentioned in the calculation details that the product for each ethylene insertion step along the reaction path showed an apparent chain rotation from a γ-agostic structure (**X**$_\gamma$) to a more stable β-agostic structure (**X**$_\beta$). This result is consistent with the ethylene insertion products in the chromium catalyst system $CrCl(H_2O)CH_3^+$ studied by Vidar R. Jensen and Knut J. Børve.[38] For model **K**, $[(\eta^6\text{-toluene})Cr(II)Me]^+$, the primary product, **6K**$_\gamma$, of ethylene insertion into the Cr−C in **5K** is a γ-agostic complex, and it forms a five-membered ring in which adjacent carbon atoms adopt staggered conformations, as shown in Figure 8. Then, the γ-

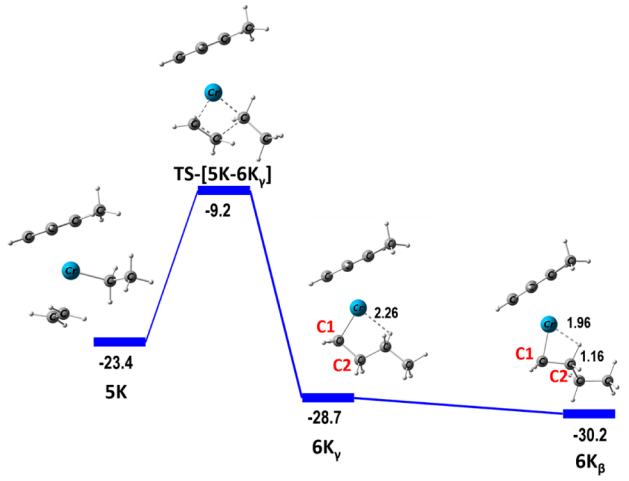

Figure 8. Gibbs free-energy profile and geometries of stationary points of ethylene insertion into the Cr−C in **5K**. **6K**$_\gamma$ and **6K**$_\beta$ are the γ-agostic and β-agostic products, respectively. Bond distances are in angstroms; Gibbs free energies are in kcal/mol.

agostic product **6K**$_\gamma$ immediately rearranges to its most stable structure of the β-agostic product **6K**$_\beta$, corresponding to a rotation along the axis of bond C1−C2. The β-agostic structure **6K**$_\beta$ is 1.5 kcal/mol more stable in energy than its conformer **6K**$_\gamma$, and in **6K**$_\beta$, a strong agostic structure is present (Cr−H = 1.96 Å; C2−H = 1.16 Å). We also found a similar trend for model **A** $[(Ph_3SiO)Cr^{III}Me]^+$ and **I** $[(\eta^6\text{-toluene})Cr^{III}Me_2]^+$, that β-agostic conformation **X**$_\beta$ is the more stabilized product than their corresponding γ-agostic structure.

On the basis of above DFT results, we propose that cationic trivalent model **A**, $[(Ph_3SiO)Cr^{III}Me]^+$, and model **I**, $[(\eta^6\text{-toluene})Cr^{III}(Me)_2]^+$, are the two most plausible active species for ethylene polymerization, and the cationic trivalent model **K**, $[(\eta^6\text{-toluene})Cr^{II}Me]^+$, is the most possible active species for ethylene nonselective oligomerization. Active species and their switching mechanism from ethylene polymerization to nonselective oligomerization in the **1**/MAO catalyst system are proposed in Scheme 3. Under the low Al/Cr molar ratio (Al/Cr ≤ 100), three monometallic species—$[(\eta^6\text{-toluene})_2Cr(I)]^+$, $[(Ph_3SiO)Cr(III)Me]^+$, and $[(\eta^6\text{-toluene})Cr(III)(Me)_2]^+$—might be generated by the alkylation and disproportionation reaction of complex **1** activated with MAO. Among these three species, the cationic monovalent $[(\eta^6\text{-toluene})_2Cr(I)]^+$ sandwich complex is inactive, and the other two cationic trivalent complexes could lead to ethylene polymerization. When the concentration of excess MAO is raised to Al/Cr ratios of over 200, the **1**/MAO system become catalytically active with the formation of ethylene nonselective oligomerization divalent cationic active species $[(\eta^6\text{-toluene})Cr^{II}Me]^+$.

In summary, the cationic Cr(III) species are responsible for ethylene polymerization, and the cationic Cr(II) species could be accountable for ethylene nonselective oligomerization. Considering the complexity of the **1**/MAO catalyst system, other chromium species that are irrelevant to catalysis can also

DOI: 10.1021/acscatal.5b00240
ACS Catal. 2015, 5, 3562−3574

Scheme 3. Proposal of the Active Species and Their Switching Mechanism for Ethylene Polymerization/Oligomerization in the 1/MAO Catalyst System

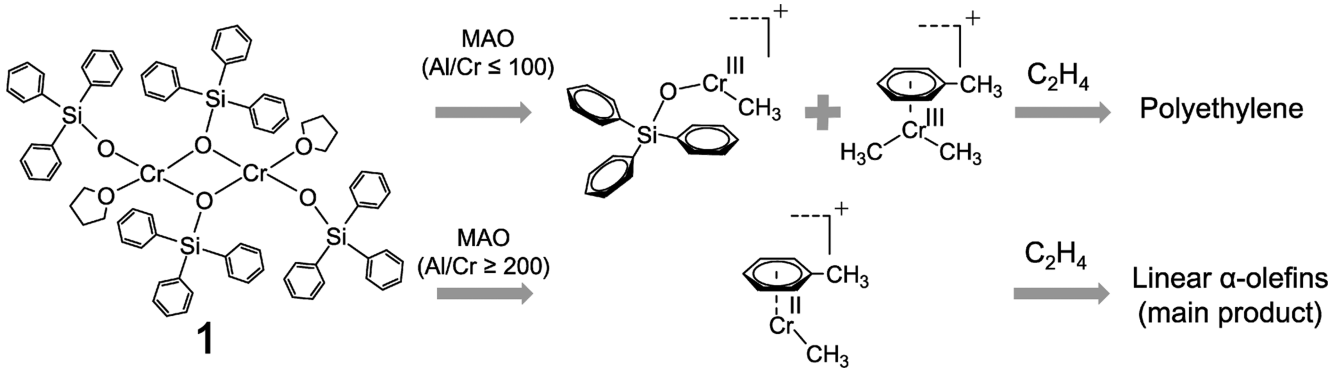

possibly exist, in addition to the real active chromium species. So there is a high possibility that the active species for ethylene nonselective oligomerization may not be necessarily generated by the ones that are responsible for ethylene polymerization. Herein, we just proposed a hypothesis that active species change with an increase in the amount of MAO, as shown in Scheme S1 in the Supporting Information. Further attempts to clarify the link between ethylene polymerization active species and nonselective oligomerization active species of the complex **1**/MAO system with combined experimental and computational methods are still in progress.

Recently, we reported that bis(triphenylsilyl)chromate, as a triphenylsiloxy complex of chromium(VI) also exhibited a similar switching behavior for ethylene polymerization/oligomerization with MAO as a cocatalyst.[78] Therefore, the similar active species and switching mechanism for ethylene polymerization/oligomerization might be also considered for the bis(triphenylsilyl)chromate/MAO catalyst system. Further experimental and theoretical investigations are still in progress.

4. CONCLUSIONS

In this work, a combined experimental and computational approach was employed to study the nature of the active chromium species and their switching mechanism between ethylene polymerization and ethylene nonselective oligomerization over the triphenylsiloxy complex of chromium(II) **1**/MAO catalyst system. The **1**/MAO catalyst system exhibited a very similar switching behavior for ethylene polymerization/oligomerization under different ethylene pressure, and the ethylene nonselective oligomerization activity was independent of ethylene pressure. It was inferred that the chain propagation and chain transfer processes proceeded via a Cossee−Arlman mechanism and β-hydrogen transfer to the chromium center, respectively. DFT calculations provided some essential insights into the nature of the active chromium species and mechanistic aspects in the **1**/MAO system. It was demonstrated that the trivalent $[(Ph_3SiO)Cr^{III}Me]^+$ and $[(\eta^6\text{-toluene})Cr^{III}Me_2]^+$ models generated from the disproportionation reaction might be the most plausible polymerization active species at lower Al/Cr ratios (≤100), and the divalent $[(\eta^6\text{-toluene})Cr^{II}Me]^+$ model was proposed to lead to ethylene nonselective oligomerization at higher Al/Cr molar ratios (≥200), which could rationally explain well the switching behavior in the **1**/MAO catalyst system.

■ ASSOCIATED CONTENT

Supporting Information

The Supporting Information is available free of charge on the ACS Publications website at DOI: 10.1021/acscatal.5b00240.

Detailed discussion about six neutral Cr(III) model and three neutral Cr(II) models, **B**, **D**, and **J**. Relative free energies of models **A**−**L** under different spin states, Gibbs free energy differences between models **C** and **I**, Gibbs free energy differences between models **E** and **K**, and energy barriers of ethylene insertion into the Cr−H bond for model $\mathbf{1X_H}$ (X = **A**, **C**, **E**, **I**, **K**). The Cartesian coordinates, total energies, and Gibbs free energies for all the complexes (PDF)

■ AUTHOR INFORMATION

Corresponding Authors

*Phone/Fax: +86-21-64253627. E-mail: boping@ecust.edu.cn.
*Phone: +972-4-8292680. Fax: +972-4-8295703. E-mail: chmoris@tx.technion.ac.il

Author Contributions

⊥J.Z. and P.Q. contributed equally to this work.

Notes

The authors declare no competing financial interest.

■ ACKNOWLEDGMENTS

National Natural Science Foundation of China (No. 20774025) and Key Projects in the National Science & Technology Pillar Program during the 11th Five-Year Plan Period (2007BAE50B04) are thanked for financial support. This work is also financially supported by the Research Program of the State Key Laboratory of Chemical Engineering, the Program of Introducing Talents of Discipline to Universities (B08021), and the Fundamental Research Funds for the Central Universities. Dr. P. Zhao (Institute of Fine Chemicals, East China University of Science and Technology) and Dr. I. Barzilai (Faculty of Chemistry, Technion-Israel Institute of Technology) are thanked for FT-IR and GC measurements, respectively.

■ REFERENCES

(1) Bordiga, S.; Groppo, E.; Agostini, G.; van Bokhoven, J. A.; Lamberti, C. *Chem. Rev.* **2013**, *113*, 1736−1850.
(2) Groppo, E.; Damin, A.; Otero Arean, C.; Zecchina, A. *Chem. - Eur. J.* **2011**, *17*, 11110−11114.
(3) Zhao, N.; Cheng, R.; He, X.; Liu, Z.; Liu, B. *Macromol. Chem. Phys.* **2014**, *215*, 1753−1766.

DOI: 10.1021/acscatal.5b00240
ACS Catal. 2015, 5, 3562−3574

(4) Gibson, V. C.; Spitzmesser, S. K. *Chem. Rev.* **2003**, *103*, 283−315.
(5) Conley, M. P.; Delley, M. F.; Siddiqi, G.; Lapadula, G.; Norsic, S.; Monteil, V.; Safonova, O. V.; Copéret, C. *Angew. Chem.* **2014**, *126*, 1903−1907.
(6) Zhong, L.; Lee, M.-Y.; Liu, Z.; Wanglee, Y.-J.; Liu, B.; Scott, S. L. *J. Catal.* **2012**, *293*, 1−12.
(7) Clark, A.; Hogan, J. P.; Witt, D. R.; Lanning, W. C. *Proc. World Pet. Congr.* **1959**, *4*, 267.
(8) Groppo, E.; Lamberti, C.; Bordiga, S.; Spoto, G.; Zecchina, A. *Chem. Rev.* **2005**, *105*, 115−184.
(9) McDaniel, M. P. *Adv. Catal.* **1985**, *33*, 47−98.
(10) McDaniel, M. P. *Adv. Catal.* **2010**, *53*, 123−606.
(11) Carrick, W. L.; Turbett, R. J.; Karol, F. J.; Karapinka, G. L.; Fox, A. S.; Johnson, R. N. *J. Polym. Sci., Part A-1: Polym. Chem.* **1972**, *10*, 2609−2620.
(12) Dixon, J. T.; Green, M. J.; Hess, F. M.; Morgan, D. H. *J. Organomet. Chem.* **2004**, *689*, 3641−3668.
(13) Arlman, E. J.; Cossee, P. *J. Catal.* **1964**, *3*, 99−104.
(14) Cossee, P. *J. Catal.* **1964**, *3*, 80−88.
(15) Manyik, R. M.; Walker, W. E.; Wilson, T. P. *J. Catal.* **1977**, *47*, 197−209.
(16) Briggs, J. R. *J. Chem. Soc., Chem. Commun.* **1989**, *1989*, 674−675.
(17) Jabri, A.; Mason, C. B.; Sim, Y.; Gambarotta, S.; Burchell, T. J.; Duchateau, R. *Angew. Chem., Int. Ed.* **2008**, *47*, 9717−9721.
(18) Tomov, A. K.; Chirinos, J. J.; Jones, D. J.; Long, R. J.; Gibson, V. C. *J. Am. Chem. Soc.* **2005**, *127*, 10166−10167.
(19) Tomov, A. K.; Chirinos, J. J.; Long, R. J.; Gibson, V. C.; Elsegood, M. R. *J. Am. Chem. Soc.* **2006**, *128*, 7704−7705.
(20) Albahily, K.; Koc, E.; Al-Baldawi, D.; Savard, D.; Gambarotta, S.; Burchell, T. J.; Duchateau, R. *Angew. Chem., Int. Ed.* **2008**, *47*, 5816−5819.
(21) Vidyaratne, I.; Nikiforov, G. B.; Gorelsky, S. I.; Gambarotta, S.; Duchateau, R.; Korobkov, I. *Angew. Chem., Int. Ed.* **2009**, *48*, 6552−6556.
(22) Dulai, A.; de Bod, H.; Hanton, M. J.; Smith, D. M.; Downing, S.; Mansell, S. M.; Wass, D. F. *Organometallics* **2009**, *28*, 4613−4616.
(23) Albahily, K.; Fomitcheva, V.; Gambarotta, S.; Korobkov, I.; Murugesu, M.; Gorelsky, S. I. *J. Am. Chem. Soc.* **2011**, *133*, 6380−6387.
(24) Albahily, K.; Shaikh, Y.; Sebastiao, E.; Gambarotta, S.; Korobkov, I.; Gorelsky, S. I. *J. Am. Chem. Soc.* **2011**, *133*, 6388−6395.
(25) Licciulli, S.; Albahily, K.; Fomitcheva, V.; Korobkov, I.; Gambarotta, S.; Duchateau, R. *Angew. Chem., Int. Ed.* **2011**, *50*, 2346−2349.
(26) Albahily, K.; Licciulli, S.; Gambarotta, S.; Korobkov, I.; Chevalier, R.; Schuhen, K.; Duchateau, R. *Organometallics* **2011**, *30*, 3346−3352.
(27) Theopold, K. H. *Eur. J. Inorg. Chem.* **1998**, *131*, 15−24.
(28) MacAdams, L. A.; Buffone, G. P.; Incarvito, C. D.; Rheingold, A. L.; Theopold, K. H. *J. Am. Chem. Soc.* **2005**, *127*, 1082−1083.
(29) Theopold, K. H. *Acc. Chem. Res.* **1990**, *23*, 263−270.
(30) Thomas, B. J.; Theopold, K. H. *J. Am. Chem. Soc.* **1988**, *110*, 5902−5903.
(31) Thomas, B. J.; Noh, S. K.; Schulte, G. K.; Sendlinger, S. C.; Theopold, K. H. *J. Am. Chem. Soc.* **1991**, *113*, 893−902.
(32) Jabri, A.; Crewdson, P.; Gambarotta, S.; Korobkov, I.; Duchateau, R. *Organometallics* **2006**, *25*, 715−718.
(33) Albahily, K.; Al-Baldawi, D.; Gambarotta, S.; Koç, E.; Duchateau, R. *Organometallics* **2008**, *27*, 5943−5947.
(34) Albahily, K.; Fomitcheva, V.; Shaikh, Y.; Sebastiao, E.; Gorelsky, S. I.; Gambarotta, S.; Korobkov, I.; Duchateau, R. *Organometallics* **2011**, *30*, 4201−4210.
(35) Temple, C.; Jabri, A.; Crewdson, P.; Gambarotta, S.; Korobkov, I.; Duchateau, R. *Angew. Chem.* **2006**, *118*, 7208−7211.
(36) Qiu, P.; Cheng, R.; Liu, B.; Tumanskii, B.; Batrice, R. J.; Botoshansky, M.; Eisen, M. S. *Organometallics* **2011**, *30*, 2144−2148.
(37) Chen, E. Y.-X.; Marks, T. J. *Chem. Rev.* **2000**, *100*, 1391−1434.
(38) Jensen, V. R.; Børve, K. J. *Organometallics* **1997**, *16*, 2514−2522.
(39) Jensen, V. R.; Angermund, K.; Jolly, P. W.; Børve, K. J. *Organometallics* **2000**, *19*, 403−410.
(40) Janse van Rensburg, W.; van den Berg, J.-A.; Steynberg, P. J. *Organometallics* **2007**, *26*, 1000−1013.
(41) Qi, Y.; Dong, Q.; Zhong, L.; Liu, Z.; Qiu, P.; Cheng, R.; He, X.; Vanderbilt, J.; Liu, B. *Organometallics* **2010**, *29*, 1588−1602.
(42) Liu, Z.; Zhong, L.; Yang, Y.; Cheng, R.; Liu, B. *J. Phys. Chem. A* **2011**, *115*, 8131−8141.
(43) Yang, Y.; Liu, Z.; Zhong, L.; Qiu, P.; Dong, Q.; Cheng, R.; Vanderbilt, J.; Liu, B. *Organometallics* **2011**, *30*, 5297−5302.
(44) Kirillov, E.; Roisnel, T.; Razavi, A.; Carpentier, J.-F. o. *Organometallics* **2009**, *28*, 2401−2409.
(45) Frisch, M. J.; Trucks, G. W.; Schlegel, H. B.; Scuseria, G. E.; Robb, M. A.; Cheeseman, J. R.; Scalmani, G.; Barone, V.; Mennucci, B.; Petersson, G. A.; Nakatsuji, H.; Caricato, M.; Li, X.; Hratchian, H. P.; Izmaylov, A. F.; Bloino, J.; Zheng, G.; Sonnenberg, J. L.; Hada, M.; Ehara, M.; Toyota, K.; Fukuda, R.; Hasegawa, J.; Ishida, M.; Nakajima, T.; Honda, Y.; Kitao, O.; Nakai, H.; Vreven, T.; Montgomery, J. A.; Peralta, J. E.; Ogliaro, F.; Bearpark, M.; Heyd, J. J.; Brothers, E.; Kudin, K. N.; Staroverov, V. N.; Kobayashi, R.; Normand, J.; Raghavachari, K.; Rendell, A.; Burant, J. C.; Iyengar, S. S.; Tomasi, J.; Cossi, M.; Rega, N.; Millam, J. M.; Klene, M.; Knox, J. E.; Cross, J. B.; Bakken, V.; Adamo, C.; Jaramillo, J.; Gomperts, R.; Stratmann, R. E.; Yazyev, O.; Austin, A. J.; Cammi, R.; Pomelli, C.; Ochterski, J. W.; Martin, R. L.; Morokuma, K.; Zakrzewski, V. G.; Voth, G. A.; Salvador, P.; Dannenberg, J. J.; Dapprich, S.; Daniels, A. D.; Farkas, O.; Foresman, J. B.; Ortiz, J. V.; Cioslowski, J.; Fox, D. J. *Gaussian09*; Gaussian: Wallingford, CT, 2009.
(46) Becke, A. D. *J. Chem. Phys.* **1993**, *98*, 5648.
(47) Becke, A. D. *J. Chem. Phys.* **1993**, *98*, 1372.
(48) Lee, C.; Yang, W.; Parr, R. G. *Phys. Rev. B: Condens. Matter Mater. Phys.* **1988**, *37*, 785−789.
(49) Fukui, K. *Acc. Chem. Res.* **1981**, *14*, 363−368.
(50) Tomasi, J.; Persico, M. *Chem. Rev.* **1994**, *94*, 2027−2094.
(51) Tomasi, J.; Mennucci, B.; Cammi, R. *Chem. Rev.* **2005**, *105*, 2999−3093.
(52) Grimme, S.; Antony, J.; Ehrlich, S.; Krieg, H. *J. Chem. Phys.* **2010**, *132*, 154104.
(53) Ehrlich, S.; Moellmann, J.; Grimme, S. *Acc. Chem. Res.* **2012**, *46*, 916−926.
(54) Brandenburg, J. G.; Alessio, M.; Civalleri, B.; Peintinger, M. F.; Bredow, T.; Grimme, S. *J. Phys. Chem. A* **2013**, *117*, 9282−9292.
(55) Brandenburg, J. G.; Grimme, S. *Top. Curr. Chem.* **2014**, *345*, 1−23.
(56) Lohrenz, J. C. W.; Woo, T. K.; Ziegler, T. *J. Am. Chem. Soc.* **1995**, *117*, 12793−12800.
(57) Döhring, A.; Jensen, V. R.; Jolly, P. W.; Thiel, W.; Weber, J. C. *Organometallics* **2001**, *20*, 2234−2245.
(58) McGuinness, D. S.; Wasserscheid, P.; Keim, W.; Morgan, D.; Dixon, J. T.; Bollmann, A.; Maumela, H.; Hess, F.; Englert, U. *J. Am. Chem. Soc.* **2003**, *125*, 5272−5273.
(59) Tang, S.; Liu, Z.; Yan, X.; Li, N.; Cheng, R.; He, X.; Liu, B. *Appl. Catal., A* **2014**, *481*, 39−48.
(60) Wang, L.; Yuan, Y.; Feng, L.; Wang, Y.; Pan, J.; Ge, C.; Ji, B. *Eur. Polym. J.* **2000**, *36*, 851.
(61) Yang, S. Y.; Ziegler, T. *Organometallics* **2006**, *25*, 887−990.
(62) Klesing, A.; Bettonville, S. *Phys. Chem. Chem. Phys.* **1999**, *1*, 2373−2377.
(63) Margl, P. M.; Woo, T. K.; Ziegler, T. *Organometallics* **1998**, *17*, 4997−5002.
(64) Rappé, A. K.; Skiff, W. M.; Casewit, C. J. *Chem. Rev.* **2000**, *100*, 1435−1456.
(65) Kaminsky, W.; Strübel, C. *J. Mol. Catal. A: Chem.* **1998**, *128*, 191−200.
(66) Kaminsky, W. *Macromol. Chem. Phys.* **1996**, *197*, 3907−3945.
(67) Tritto, I.; Li, S.; Sacchi, M. C.; Zannoni, G. *Macromolecules* **1993**, *26*, 7111−7115.
(68) Tritto, I.; Li, S. X.; Sacchi, M. C.; Locatelli, P.; Zannoni, G. *Macromolecules* **1995**, *28*, 5358−5362.

DOI: 10.1021/acscatal.5b00240
ACS Catal. 2015, 5, 3562−3574

(69) Calderazzo, F.; Englert, U.; Pampaloni, G.; Volpe, M. *J. Organomet. Chem.* **2005**, *690*, 3321−3332.
(70) Köhn, R. D.; Smith, D.; Mahon, M. F.; Prinz, M.; Mihan, S.; Kociok-Köhn, G. *J. Organomet. Chem.* **2003**, *683*, 200−208.
(71) Espelid, Ø.; Børve, K. J. *J. Catal.* **2000**, *195*, 125−139.
(72) Espelid, Ø.; Børve, K. J. *J. Catal.* **2002**, *205*, 366−374.
(73) La Macchia, G.; Gagliardi, L.; Power, P. P.; Brynda, M. *J. Am. Chem. Soc.* **2008**, *130*, 5104−5114.
(74) Kreisel, K. A.; Yap, G. P. A.; Dmitrenko, O.; Landis, C. R.; Theopold, K. H. *J. Am. Chem. Soc.* **2007**, *129*, 14162−14163.
(75) Tsai, Y.-C.; Wang, P.-Y.; Chen, S.-A.; Chen, J.-M. *J. Am. Chem. Soc.* **2007**, *129*, 8066−8067.
(76) Liu, Z.; Somsook, E.; White, C. B.; Rosaaen, K. A.; Landis, C. R. *J. Am. Chem. Soc.* **2001**, *123*, 2915−2916.
(77) Talarico, G.; Blok, A. N. J.; Woo, T. K.; Cavallo, L. *Organometallics* **2002**, *21*, 4939−4949.
(78) Qiu, P.; Cheng, R.; Liu, Z.; Liu, B.; Tumanskii, B.; Eisen, M. S. *J. Organomet. Chem.* **2012**, *699*, 48−55.

DOI: 10.1021/acscatal.5b00240
ACS Catal. 2015, 5, 3562−3574